Volt-Var Optimization with Power Management of Plug-in Electric Vehicles for Conservation Voltage Reduction in Distribution Systems

Darwin A. Quijano, Antonio Padilha-Feltrin, *Senior Member, IEEE,* and João P. S. Catalão, *Fellow, IEEE.*

***Abstract*—This paper addresses the problem of Volt-Var optimization for conservation voltage reduction (CVR) implementation in medium voltage electric distribution systems (EDS) with high penetration of renewable energy sources (RES)-based distributed generation (DG) and plug-in electric vehicles (EVs). The proposed strategy seeks to coordinate the power dispatch of aggregated electric vehicles (EVs) for EDS voltage regulation taking into account technical characteristics and the driving patterns of individual EVs. Active and reactive V2G capabilities of EV chargers are harnessed to enhance the capacity for voltage regulation and energy savings. The strategy is for the day-ahead operation scheduling, where decisions are made based on predictions of RES-based DG power production, conventional load consumption and EV driving patterns. Forecast errors are taken into account through a two-stage stochastic programming formulation, where probability density functions are used to describe the uncertainties of predicted parameters. Simulations were carried out on a 33-bus test system and results showed energy savings of up to 4.14% when EVs participate in voltage control.**

***Index Terms*—Conservation voltage reduction, electric vehicles, renewable energy sources.**

I. Introduction

Conservation voltage reduction (CVR) is the procedure of reducing the voltage levels in electric distribution systems (EDSs) to induce a reduction in the consumption of voltage dependent loads [1]. It is a demand response resource available to distribution system operators (DSOs) as long as the EDS voltage levels can be reduced within the statutory limits. However, regulating voltage in EDSs with a significant amount of renewable energy sources (RES)-based distributed generation (DG) is challenging because of the variability and unpredictability of power production.

Voltage regulation for CVR implementation in EDSs has traditionally been performed using legacy devices such as on-load tap changers (OLTCs), distributed voltage regulators, and capacitor banks. A common approach involves controlling the OLTC through a line drop compensation method to reduce the substation's secondary voltage [2]. Using this method, field tests have reported 0.3% to 1% load reduction per 1% voltage reduction [3]. Upgrading computation and communication technologies in modern EDSs has enabled the integration of CVR into Volt-Var optimization (VVO) models, increasing the CVR gains [1], [4]. A VVO model can optimally coordinate the operation of multiple Volt-Var control devices to achieve one or more EDS operating objectives, making it an effective way to improve the implementation of CVR [5].

The voltage regulation capability of traditional Volt-Valt control devices is restricted by their slow time response, discrete features, and limited number of switching operations. These drawbacks limit the potential benefits of CVR in EDSs with high penetration of RES-based DG, given the fast and unpredictable voltage fluctuations. Therefore, to improve CVR performance, modern VVO models have been developed, incorporating optimal control of fast-response technologies such as PV smart inverters [6], [7], battery energy storage systems [8], [9], demand response [10], and static synchronous compensators [11]. Additionally, to account for uncertainties of RES-based DG power production and load demand, optimization under uncertainty techniques such as stochastic programming have been utilized [7], [12].

Given the increasing penetration of plug-in electric vehicles (EVs) in EDSs, optimal EV charging coordination has been proposed as a solution for the optimized EDSs operation [13]. Further, EVs can function as vehicle-to-grid (V2G) devices by injecting power back into the EDS, enabling the provision of ancillary services and promoting the integration of renewable energy. For example, a rolling prediction-decision framework is proposed in [14] for EVs to provide load shifting service. In [15] valley-filling and peak-shaving of the load curve is procured by coordinating the charging/discharging of EVs through a decentralized scheduling scheme. The authors of [16] propose game theoretic approaches to motivate EVs to provide frequency regulation. Coordinated charging/discharging dispatch of EVs is proposed in [17] as a solution to increase the hosting capacity of RES-based DG in EDSs.

New possibilities for V2G applications have been revealed as the power electronic inverters used to charge the EV batteries have been shown to have the potential to provide reactive power compensation [18]. Building on this finding, Hu *et al.* [19] propose the utilization of reactive power dispatch from EVs to minimize the energy losses in EDSs. In addition, the ability of V2G-enabled EV chargers to compensate reactive power is exploited through a strategy for real-time voltage regulation in [20].

This work was supported by São Paulo Research Foundation (FAPESP) under grants: 2018/06451-8, 2020/12401-3 and 2015/21972-6, by CNPq under grant: 310299/2020-9, and by CAPES (code finance 001).

D.A. Quijano and A. Padilha-Feltrin are with Universidade Estadual Paulista–UNESP, Ilha Solteira 15385-000, Brazil (e-mail: alexisqr@yahoo.es; antonio.padilha-feltrin@unesp.br).

J. P. S Catalão is with the Faculty of Engineering of the University of Porto (FEUP) and INESC TEC, 4200-465, Porto, Portugal (e-mail: catalao@fe.up.pt).

Nevertheless, only a few works have investigated the implementation of CVR in EDSs with EVs [21]–[24]. In [21], [23] the reactive power injection from EV charging stations is optimally controlled to influence the voltage profile and, consequently, the power consumption of voltage-dependent loads. However, these works do not address the optimal EV charging strategy for voltage regulation or consider the active and reactive V2G capabilities of dispersed EV chargers connected to any outlet available at home garages or workplaces. In contrast, Gharavi *et al.* [22] propose an optimized EV charging dispatch strategy for CVR implementation, however, without considering reactive power compensation from EV chargers and the presence of RES-based DG in the EDS. The strategy proposed in [24] considers the presence of RES-based DG in the EDS when implementing CVR by adopting the optimal charging of EVs. However, it also fails to exploit the potential reactive power capability of the EV chargers. Furthermore, the uncertainties associated with EV driving patterns are not taken into account in [21]–[23].

To address the gap in the current literature, this work addresses the problem of implementing CVR in medium voltage (MV) EDSs taking advantage of the active and reactive V2G capabilities of EV chargers. Large populations of dispersed EVs are modeled through an aggregation strategy that takes into account technical specifications and driving patterns of individual EVs. The VVO problem is formulated from the point of view of the DSO who centrally decides the active and reactive power dispatch of the EVs aggregated at specific EDS buses. The strategy is for the day-ahead operation scheduling, where decisions are made based on predictions of RES-based DG power production, conventional load consumption, and EV driving patterns. Moreover, prediction errors are taken into account through a two-stage stochastic programming formulation.

The contributions of this work are summarized as follows:

- A novel strategy that takes advantage of the controllability of EVs (including active and reactive V2G capabilities) for CVR implementation in MV EDSs with high penetration of RES-based DG.
- An aggregation strategy developed to exploit the aggregated active and reactive V2G capabilities of large populations of dispersed EVs for voltage regulation.
- A VVO model formulated as a two-stage stochastic programming problem to coordinate the dispatch of aggregated EVs and the OLTC operation for CVR implementation. This formulation is proposed to simultaneously take into account uncertainties of RES-based DG power production (including solar PV and wind), conventional load consumption, and EVs driving patterns in the CVR problem, which has not been done before.

II. Mathematical model

This section presents the mathematical formulation that models the problem of controlling the voltage levels for energy conservation in EDSs. The problem is formulated for the day-ahead operation scheduling of EDSs, and uncertainties are taken into account adopting a two-stage stochastic programming formulation. First-stage decisions correspond to the OLTC tap settings for each hour of the next day, which must hold for all possible uncertainty realizations because of their slow response and discrete nature. The active and reactive powers absorbed and injected by the EVs aggregated at specific buses correspond to the second-stage decisions, which are adjusted according to the uncertainty realizations. Prediction errors of RES-based DG power production, conventional demand, and EV driving patterns are characterized using PDFs from which a set of representative scenarios (uncertainty realizations) is sampled. In the following formulation the indices $s \in \Omega_s$, $t \in \Omega_t$, $i \in \Omega_b$, and $ij \in \Omega_l$ correspond to scenarios, hours, buses, and line segments, respectively. Ω_s, Ω_t, Ω_b, and Ω_l denote the sets of scenarios, hours, buses and line segments.

A. Objective function

The objective function is formulated to minimize the expected value of the energy consumption of voltage dependent loads plus the energy losses in distribution lines during the day as follows:

$$min: \sum_{s\in\Omega_s} \rho_s \sum_{t\in\Omega_t} \tau \left(\sum_{i\in\Omega_b} P^l_{i,t,s} + \sum_{ij\in\Omega_l} r_{ij} I^{sqr}_{ij,t,s} \right). \quad (1)$$

where, ρ_s, $P^l_{i,t,s}$, r_{ij}, and $I^{sqr}_{ij,t,s}$ denote the scenario probability, conventional load active power, resistance of line segments, and magnitude of the current squared in line segments. τ indicates the duration of the time interval, which in this work is equal to one hour.

B. Voltage dependent loads

The voltage dependent behavior of loads is modeled using the ZIP model as follows:

$$P^l_{i,t,s} = P^Z_{i,t,s} V^2_{i,t,s} + P^I_{i,t,s} V_{i,t,s} + P^P_{i,t,s}, \quad (2)$$

$$Q^l_{i,t,s} = Q^Z_{i,t,s} V^2_{i,t,s} + Q^I_{i,t,s} V_{i,t,s} + Q^P_{i,t,s}. \quad (3)$$

This model describes conventional loads as a combination of constant impedance (Z), constant current (I), and constant power (P) components. The participation of each component in the total load active (reactive) power is given by $P^Z_{i,t,s}$, $P^I_{i,t,s}$, and $P^P_{i,t,s}$ ($Q^Z_{i,t,s}$, $Q^I_{i,t,s}$, and $Q^P_{i,t,s}$). These components are uncertain parameters modeled through PDFs as will be shown later. $Q^l_{i,t,s}$ and $V_{i,t,s}$ denote the conventional load reactive power and the magnitude of the bus voltage, respectively.

C. Distributed generation

This work considers the presence of solar PV and wind-based DG in the EDS. The active power supplied by these generation technologies is given by

$$P^w_{i,t,s} = \omega^w_{t,s} S^w_i, \quad (4)$$

$$P^{pv}_{i,t,s} = \omega^{pv}_{t,s} S^{pv}_i, \quad (5)$$

where, $P^w_{i,t,s}$ and $P^{pv}_{i,t,s}$ indicate the active power supplied by the wind-based DG and the solar PV-based DG, respectively.

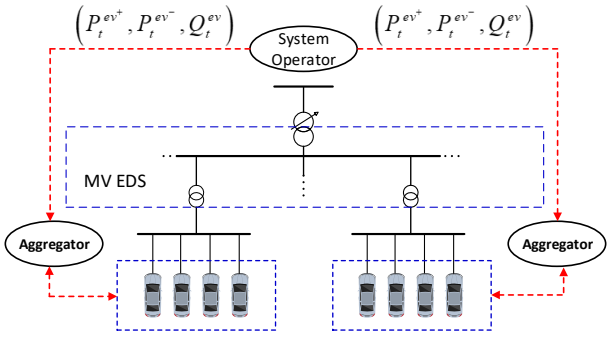

Fig. 1: Schematic of EV coordination in the EDS.

$\omega_{t,s}^{w}$ and $\omega_{t,s}^{pv}$ denote the normalized active power of the wind-based DG and the solar PV-based DG, respectively. These are uncertain parameters described by PDFs as will be shown in the next section. S_i^{w} and S_i^{pv} are the rated capacity of the wind-based DG and solar PV-based DG, respectively.

D. Aggregated EV model

The proposed approach takes advantage of the controllability of EVs to regulate bus voltages and induce a reduction in the energy consumption of voltage dependent loads and energy losses. The coordination of the dispatch of large populations of dispersed EVs is achieved through the adoption of a hierarchical control architecture, as illustrated in Fig. 1. In this architecture, the DSO centrally determines the active and reactive powers that need to be absorbed and injected into the MV EDS by the EVs aggregated at each node and time interval. Aggregators are responsible for estimating the dispatch of individual EVs, in a way that satisfies the requirements of the DSO, while also ensuring that the energy needs of all EVs are met.

The scope of this work is restricted to the VVO problem that coordinates the dispatch of the aggregated EVs, and the issue of coordinating the dispatch of individual EVs by the aggregators is not addressed. This approach is possible because it is considered that the DSO schedules the power to be injected and absorbed by the aggregated EVs at each node and time interval aware of the number of EVs plugged in and their state of charge (SOC). This information is forecasted by the DSO to model each aggregated collection of EVs as a virtual storage device whose power and energy capacities are uncertain and dynamic [17]. Thus, the DSO dispatches the aggregated EVs taking into account their capacity bounds and the energy requirements of individual EVs. The dispatch of the aggregated EVs is modeled as follows:

$$E_{i,t,s} = E_{i,t-1,s} + E_{i,t,s}^{arr} - E_{i,t,s}^{dep} + \eta^{+}\tau P_{i,t,s}^{ev^+} - \frac{1}{\eta^{-}}\tau P_{i,t,s}^{ev^-}, \quad (6)$$

$$0 \le E_{i,t,s} \le E_{i,t,s}^{\max}, \quad (7)$$

$$0 \le P_{i,t,s}^{ev^+} \le z_{i,t,s}^{+}\overline{S}_{i,t,s}^{ev}, \quad (8)$$

$$0 \le P_{i,t,s}^{ev^-} \le z_{i,t,s}^{-}\overline{S}_{i,t,s}^{ev}, \quad (9)$$

$$z_{i,t,s}^{-} + z_{i,t,s}^{+} \le 1, \quad (10)$$

$$(P_{i,t,s}^{ev^+} + P_{i,t,s}^{ev^-})^2 + (Q_{i,t,s}^{ev})^2 \le (\overline{S}_{i,t,s}^{ev})^2, \quad (11)$$

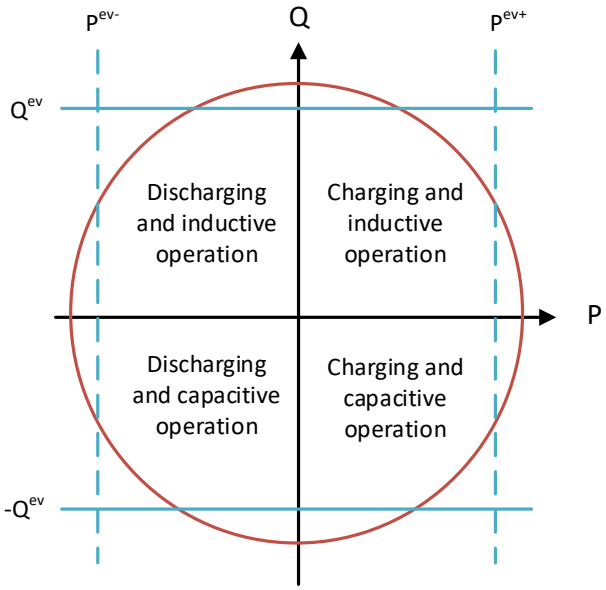

Fig. 2: Capability curve of aggregated EV chargers.

where, (6) models the dynamic energy balance of the aggregated EVs. The energy stored by the EVs aggregated at bus i ($E_{i,t,s}$) at each time interval t depends on the energy stored at the previous time interval $t-1$ ($E_{i,t-1,s}$), the energy increase due to EVs arriving ($E_{i,t,s}^{arr}$), the energy drop due to EVs departing ($E_{i,t,s}^{dep}$), the energy absorbed from the EDS ($\eta^{+}\tau P_{i,t,s}^{ev^+}$) and the energy injected into the EDS ($\tau P_{i,t,s}^{ev^-}/\eta^{-}$). η^{+} and η^{-} indicate the charging and discharging efficiencies of individual EVs. The stored energy ($E_{i,t,s}$), power absorbed by the aggregated EVs ($P_{i,t,s}^{ev^+}$), and power injected by the aggregated EVs ($P_{i,t,s}^{ev^-}$) are constrained in (7)-(9) to minimum and maximum values. $E_{i,t,s}^{\max}$ and $\overline{S}_{i,t,s}^{ev}$ indicate the maximum storage capacity and the apparent power capacity of the chargers of the aggregated EVs, respectively. The binary variables $z_{i,t,s}^{-}$ and $z_{i,t,s}^{+}$ define the operation status of the aggregated EVs. Constraint (10) prevents the EVs to absorb and inject power simultaneously. Constraint (11) describes the capability curve of the aggregated EV chargers. From this constraint it is observed that the available reactive power is determined by the chargers' apparent power and the active power injected or absorbed by the aggregated EVs. In this formulation, $Q_{i,t,s}^{ev}$ denotes the reactive power supplied by the aggregated EVs.

The capability curve of the aggregated EV chargers is shown in Fig. 2. The aggregated EV chargers can operate absorbing active power in inductive or capacitive mode ($P>0$, $Q>0$ or $Q<0$), and injecting active power in inductive or capacitive mode ($P<0$, $Q>0$ or $Q<0$). In addition, the aggregated EV chargers can only absorb or inject active power ($P>0$ or $P<0$, $Q=0$), and can only absorb or inject reactive power ($P=0$, $Q>0$, $Q<0$). It should be noted that the reactive power V2G ability of a charger can be ensured by installing a capacitor at the DC side of the inverter. This ensures that the EV battery is not involved in the exchange of reactive power [18].

The power and energy limits of the EVs aggregated at bus i, for each time interval t and scenario s, are calculated taking into account the connection status and SOC of every EV as follows:

$$E^{\max}_{i,t,s} = \sum_{m \in M_i} E^{cap}_m f_{m,t,s}, \tag{12}$$

$$\overline{S}^{ev}_{i,t,s} = \sum_{m \in M_i} \hat{S}^{ev}_m f_{m,t,s}, \tag{13}$$

$$E^{arr}_{i,t,s} = \sum_{m \in M_i} E^{ini}_{m,s} g^{arr}_{m,t,s}, \tag{14}$$

$$E^{dep}_{i,t,s} = \sum_{m \in M_i} E^{cap}_m g^{dep}_{m,t,s}, \tag{15}$$

where, (12) calculates the maximum storage capacity of the aggregated EVs as the sum of the battery capacities of individual EVs (E^{cap}_m). (13) calculates the apparent power capacity of the aggregated EV chargers as the sum of the apparent power capacities ($\hat{S}^{ev}_m$) of individual EV chargers. $f_{m,t,s}$ is a binary parameter that indicates if an EV m is plugged into the EDS at time interval t and scenario s. The value taken by $f_{m,t,s}$ is determined by the times when the EV m arrives ($t^{arr}_{m,s}$) and departs ($t^{dep}_{m,s}$). $t^{arr}_{m,s}$ and $t^{dep}_{m,s}$ are uncertain parameters modeled using PDFs as will by shown in the following section. M_i indicates the set of EVs aggregated at bus i.

Constraints (14) and (15) determine the increase and decrease in the energy stored by the aggregated EVs due to EVs arriving and departing at time t, respectively. The binary parameter $g^{arr}_{m,t,s}$ in (14) takes the value 1 at time interval $t^{arr}_{m,s}$ when the EV m arrives and is plugged in, and takes the value 0 at other time intervals. In (15), the binary parameter $g^{dep}_{m,t,s}$ takes the value 1 at time interval $t^{dep}_{m,s}$ when the EV m is plugged out and departs, and takes the value 0 at other time intervals. The SOC $E^{ini}_{m,s}$ of the EV m at the arriving time is determined by the consumption per mile and the daily travel mileage ($\chi_{m,s}$), which is an uncertain parameter modeled using a PDF. Constraint (15) establishes that EVs depart with the battery at full capacity E^{cap}_m.

E. OLTC model

The model adopted for the OLTC is defined as follows:

$$V_{i,t,s} = \tilde{V}_{i,t,s} + \Delta tap_i tap_{i,t}, \tag{16}$$

$$-\overline{tap}_i \le tap_{i,t} \le \overline{tap}_i, \tag{17}$$

$$\lambda^R_{i,t} \ge tap_{i,t+1} - tap_{i,t}, \tag{18}$$

$$\lambda^R_{i,t} \ge tap_{i,t} - tap_{i,t+1}, \tag{19}$$

$$\sum_{t \in \Omega_t} \lambda^R_{i,t} \le N^{tp}_i. \tag{20}$$

In the above formulation, (16) indicates that the voltage $V_{i,t,s}$ at the regulated end of the OLTC is equal to the voltage $\tilde{V}_{i,t,s}$ at the non-regulated end plus the adjustment $\Delta tap_i tap_{i,t}$. Δtap_i denotes the step of voltage variation per switching operation, and $tap_{i,t}$ the tap position, which is an integer control variable that must hold for all scenarios s. Constraint (17) defines the range of variation of the tap position, limited by minimum ($-\overline{tap}_i$) and maximum ($\overline{tap}_i$) values. The number of switching operation of the OLTC during the day are limited to a maximum value N^{tp}_i in (18)-(20). In this formulation, $\lambda^R_{i,t}$ is an auxiliary variable that indicates the number of switching operations between the two consecutive time intervals.

F. Power balance equations

The power power flows at each node i are described using the DistFlow equations [25] as follows:

$$\sum_{ij \in \Omega_l} P_{ij,t,s} = P_{hi,t,s} - r_{hi} I^{sqr}_{hi,t,s} - P^l_{i,t,s} - P^{ev^+}_{i,t,s} + P^{ex}_{i,t,s} + P^{ev^-}_{i,t,s} + P^w_{i,t,s} + P^{pv}_{i,t,s}, \tag{21}$$

$$\sum_{ij \in \Omega_l} Q_{ij,t,s} = Q_{hi,t,s} - x_{hi} I^{sqr}_{hi,t,s} - Q^l_{i,t,s} - Q^{ev}_{i,t,s} + Q^{ex}_{i,t,s}, \tag{22}$$

$$\tilde{V}_{j,t,s} = V_{i,t,s} - \left(r_{ij} P_{ij,t,s} + x_{ij} Q_{ij,t,s}\right) / V^{n2}. \tag{23}$$

$$I^{sqr}_{hi,t,s} = \left(P^2_{hi,t,s} + Q^2_{hi,t,s}\right) / V^{n2}. \tag{24}$$

$$\underline{V} \le V_{j,t,s} \le \overline{V}, \tag{25}$$

where, h is the node upstream node i and $j|ij \in \Omega_l$ is the set of nodes downstream node i for a distribution system with radial topology. $P_{ij,t,s}$ and $Q_{ij,t,s}$ indicate, respectively, the active and reactive power flow between buses i and j. $P^{ex}_{i,t,s}$ and $Q^{ex}_{i,t,s}$ denote, respectively, the active and reactive power exchange through the substation. x_{hi} indicates the reactance of the line segment hi. $\underline{V}$ and $\overline{V}$ are, respectively, the minimum and maximum bus voltages. V^n is the nominal voltage.

G. Model convexification

The optimization model given by (1)-(25) is mixed integer nonlinear. Nonlinearities result from constraints (2), (3) and (24), which also make the problem nonconvex. Constraints (2) and (3) are covexified by applying a linear approximation based on Taylor's expansion around $V_{i,t,s} = V^n = 1.0\ p.u.$ disregarding the second and higher order terms as follows:

$$P^l_{i,t,s} = P^Z_{i,t,s}(2V_{i,t,s} - 1) + P^I_{i,t,s} V_{i,t,s} + P^P_{i,t,s} \tag{26}$$

$$Q^l_{i,t,s} = Q^Z_{i,t,s}(2V_{i,t,s} - 1) + Q^I_{i,t,s} V_{i,t,s} + Q^P_{i,t,s} \tag{27}$$

Since the problem is formulated to maintain bus voltages within a tight range around V^n, the error introduced by the approximation (26) and (27) is not too significant. Constraint (24) is convexified by relaxing the equality as follows:

$$I^{sqr}_{hi,t,s} \ge \left(P^2_{hi,t,s} + Q^2_{hi,t,s}\right) / V^{n2}. \tag{28}$$

Sufficient conditions for this relaxation to be exact is that the bus voltage is kept close to V^n and that the power injection at each bus is not too large [26].

III. Uncertainty characterization

The proposed optimization algorithm schedules the operation of the OLTC and the dispatch of the aggregated EVs based on predictions of generation, conventional demand, and EVs travel patterns. Such predictions are subject to prediction errors, which in this work are modeled through a scenario based approach. This approach assumes that the uncertain parameters can be described by PDFs from which scenarios are sampled.

A. RES-based DG power uncertainty

The forecast errors of solar PV and wind-based DG power production are considered to be described by Beta PDFs [27]. The Beta PDF for wind-based DG is defined as follows:

$$f_{\bar{\omega}_t^w}\left(\omega_t^w\right) = \frac{\omega_t^{w\alpha_t-1}\cdot\left(1-\omega_t^w\right)^{\beta_t-1}}{B\left(\alpha_t,\beta_t\right)}, \tag{29}$$

$$B\left(\alpha_t,\beta_t\right) = \int_0^1 \omega_t^{w\alpha_t-1}\cdot\left(1-\omega_t^w\right)^{\beta_t-1} d\omega_t^w, \tag{30}$$

where, $0 \le \omega_t^w \le 1$ and $\alpha_t, \beta_t > 0$. Given a prediction of wind power $\bar{\omega}_t^w$ at time interval t, (29) models the possible uncertainty realizations ω_t^w. α_t and β_t are parameters of the Beta PDF and depend on the mean value $\bar{\omega}_t^w$ and the standard deviation σ_t according to the following expressions:

$$\alpha_t = \frac{\left(1-\bar{\omega}_t^w\right)\cdot\bar{\omega}_t^{w\,2}}{\sigma^2} - \bar{\omega}_t^w, \tag{31}$$

$$\beta_t = \frac{1-\bar{\omega}_t^w}{\bar{\omega}_t^w}\cdot\alpha_t. \tag{32}$$

The relationship between $\bar{\omega}_t^w$ and σ_t is given by $\sigma_t = 0.5\bar{\omega}_t^w(1-\bar{\omega}_t^w)$ [27]. The formulation of the Beta PDF for solar PV-based DG is the same as (29)-(32) with the variables changed accordingly.

B. Conventional load uncertainty

The forecast errors of the conventional load consumption are modeled using a normal PDF. Specifically, the possible realizations of the conventional load consumption $P_{i,t,s}^Z$, $P_{i,t,s}^I$ and $P_{i,t,s}^P$ are assumed to be normally distributed around the predicted value with a standard deviation of 2%.

C. Uncertainty of EVs

The arriving t_m^{arr} and departing t_m^{dep} times of each EV m are modeled using segmented normal distribution functions [28] as follows:

$$f_r(t_m^{dep}) = \begin{cases} \frac{1}{\sqrt{2\pi}\sigma_r}\exp\left[-\frac{\left(t_m^{dep}-\mu_r\right)^2}{2\sigma_r^2}\right], 0 < t_m^{dep} \le (\mu_r+12), \\ \frac{1}{\sqrt{2\pi}\sigma_r}\exp\left[-\frac{\left(t_m^{dep}-24-\mu_r\right)^2}{2\sigma_r^2}\right], (\mu_r+12) < t_m^{dep} \le 24, \end{cases} \tag{33}$$

$$f_e(t_m^{arr}) = \begin{cases} \frac{1}{\sqrt{2\pi}\sigma_e}\exp\left[-\frac{(t_m^{arr}+24-\mu_e)^2}{2\sigma_e^2}\right], 0 < t_m^{arr} \le (\mu_e-12), \\ \frac{1}{\sqrt{2\pi}\sigma_e}\exp\left[-\frac{(t_m^{arr}-\mu_e)^2}{2\sigma_e^2}\right], (\mu_e-12) < t_m^{arr} \le 24, \end{cases} \tag{34}$$

For each EV m, the travel mileage χ_m is described using a logarithmic normal distribution as follows:

$$f_d\left(\chi_m\right) = \frac{1}{\sqrt{2\pi}\sigma_d}\exp\left[-\frac{\left(\ln\chi_m-\mu_d\right)^2}{2\sigma_d^2}\right]. \tag{35}$$

The travel mileage χ_m is used to calculate the the SOC of the EV m at time t_m^{arr}. The shape of the PDFs (33)-(35) is defined by the following values: $\mu_r = 8.92$, $\sigma_r = 3.24$, $\mu_e = 17.47$, $\sigma_e = 3.41$, $\mu_d = 2.98$, $\sigma_d = 1.14$ [28].

D. Scenarios generation

A scenario generation and reduction process is used to obtain a set of scenarios that efficiently approximates the PDFs that model the system's uncertainties. Initially, a large set of scenarios, each with the same probability of occurrence, is sampled from the PDFs. Then, the simultaneous backward reduction technique [29] is applied to obtain a reduced set of scenarios each with probability of occurrence ρ_s. In this way, it is possible to accurately take into account uncertainties ensuring that the optimization problem can be solved using viable computational resources.

IV. Case Study and Simulations Results

This section describes the setup for the case study and discusses the simulations results. The model was implemented in the algebraic modeling language AMPL and solved using the solver CPLEX.

A. Technical data and specifications

Simulation results were obtained from a 33-bus test system whose topology is shown in Fig. 3. The conventional load and line data can be found in [25]. This EDS has peak active load consumption of 3.715 MW and nominal voltage of 12.66 kV. The substation transformer has a capacity of 5 MVA and is installed with an OLTC that is capable of regulating $\pm 5\%$ of input voltage in steps of $\Delta tap_i = 0.0125\ p.u.$ with $\overline{tap} = 4$. The number of switching operations of the OLTC during the day is limited to 16 (i.e., $N_i^{tp} = 16$). The bus voltages are limited to maximum and minimum values of 1.05 and 0.95 p.u., respectively. The participation of the constant impedance, constant current and constant power load components in the total conventional load is considered to be 40%, 40% and 20%, respectively.

Wind-based DG is installed at buses 14 and 20, both with rated capacity of 1.25 MW. Solar PV-based DG with rated capacity of 1.5 MW is installed at bus 28. This RES-based DG installed capacity represents a penetration level of 107%, determined using the definition of EV penetration level as the ratio of the total RES-based DG installed capacity to the peak demand of the conventional load. The type of EV considered is Nissan Leaf with battery capacity of 40 kWh, maximum apparent power of the charger of 7 kW, average consumption of 0.3 kWh/mi, and charging discharging efficiencies of 95% [30]. The EDS supplies a population of 318 EVs aggregated in the same proportion at buses 18, 22, 25 and 33. This population of EVs represents a 60% penetration level, calculated by adopting the definition of EV penetration level as the ratio of the total apparent power capacity of the EV chargers to the peak demand of the conventional load.

Predictions of conventional load consumption, solar PV-based DG power production, and wind-based DG power production are shown in Fig. 4. Using these predictions, 1000 scenarios are randomly generated using the PDFs presented in section III. Then, the simultaneous backward reduction technique was applied to reduce the scenario number to 10.

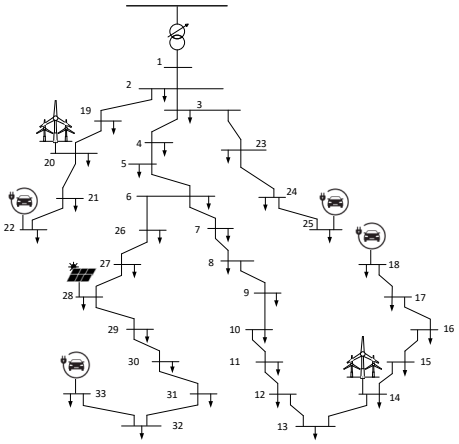

Fig. 3: Diagram of the 33-bus test system

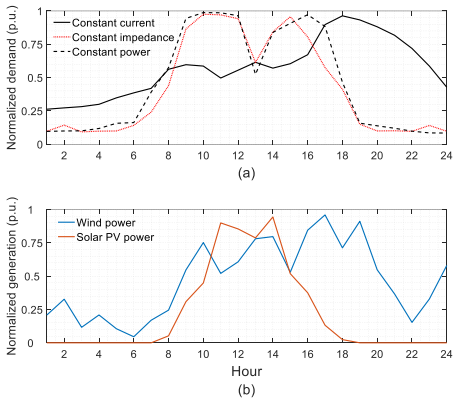

Fig. 4: Predicted profiles of a) conventional load consumption and b) Renewable-based DG production.

To asses the impact of the optimal dispatch of aggregated EVs to reduce the consumption of voltage dependent loads and the energy losses the following cases are defined:

1) Case I: OLTC operation without optimal EV active and reactive power dispatch. This case considers that the EVs are charged at maximum rate once they are plugged into the EDS.
2) Case II: OLTC operation and optimized active power absorption of aggregated EVs. This case assumes that the charging of EVs is optimally dispatched.
3) Case III: OLTC operation and optimized active power absorption and injection of aggregated EVs. This case considers EVs with V2G capability for active power.
4) Case IV: OLTC operation and optimized active and reactive power absorption and injection of aggregated EVs. This case considers EVs with V2G capability for active and reactive power.

B. Results

Since the optimization problem is evaluated over a set of scenarios, the presented power, energy and voltage results correspond to expected values over all simulated scenarios. The energy savings that can be achieved during the day through the optimal dispatch of the aggregated EVs are shown in Fig. 5. As expected, as the controllability of EVs is

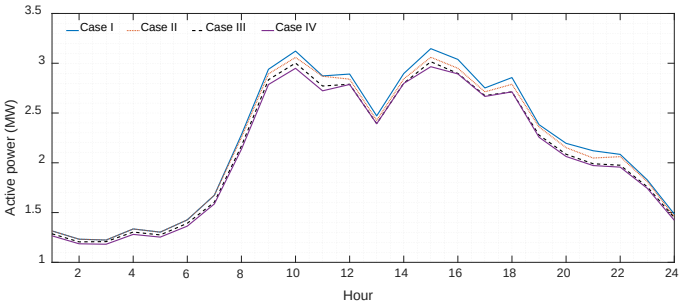

Fig. 5: Daily profiles of conventional load consumption plus energy losses.

TABLE I: Summary of the results for the day

	Case I	Case II	Case III	Case IV
Conventional load (MWh)	51.69	51.06	49.90	49.55
Losses (MWh)	1.12	1.04	0.98	0.80
Vmin (p.u.)	0.9806	0.9644	0.9500	0.9500
ΔConventional load(%)	-	1.21	3.46	4.14
ΔLosses (%)	-	7.14	12.50	28.57

increased, larger energy savings are obtained throughout the day.

A summary of the results for the 24-hour period is presented in table I. The results demonstrate that optimizing the power absorbed by the aggregated EVs in case II can reduce the energy consumption of the conventional load by 1.21% compared to case I. Moreover, the energy savings increase to 3.46% when the EVs have the ability to inject active power into the EDS in case II. Additionally, enabling both active and reactive V2G capabilities of EVs in case IV results in a reduction of 4.14% in the energy consumption. Optimally dispatching electric vehicles (EVs) provides not only a reduction in conventional load consumption but also an important advantage of minimizing energy losses. In comparison to case I, cases II, III, and IV show energy losses reductions of 7.14%, 12.50%, and 28.57%, respectively. It is important to highlight that, in all cases, voltage reductions does not compromise the supply quality for any consumers.

The active power exchanged by the EVs population at each hour for the four cases is shown in Fig. 6. Figure 7 illustrates the OLTC tap positions at each hour for the four cases. In the absence of optimal dispatch in case I, the consumption of the EV population concentrates between hours 12-24. This behavior is influenced by the battery's initial SOC and the arrival time of the EVs. In case II, the active power supplied to the EVs is shifted to the hours with higher generation. In this case, the optimized dispatch of the EVs complements the operation of the OLTC. As shown in Fig. 7, case II achieved lower tap positions than case I by controlling the active power absorbed by the EVs to flatten the net demand profile (generation minus demand) in the EDS over the day. As a result, the OLTC tap position can be lowered without requiring to increase the number of switching operations.

EVs in case III inject active power into the EDS during low generation hours and absorb active power during high generation hours. This creates a more even net demand profile compared to case II, which allows the OLTC tap to be switched

This article has been accepted for publication in IEEE Transactions on Industry Applications. This is the author's version which has not been fully edited and content may change prior to final publication. Citation information: DOI 10.1109/TIA.2023.3318582

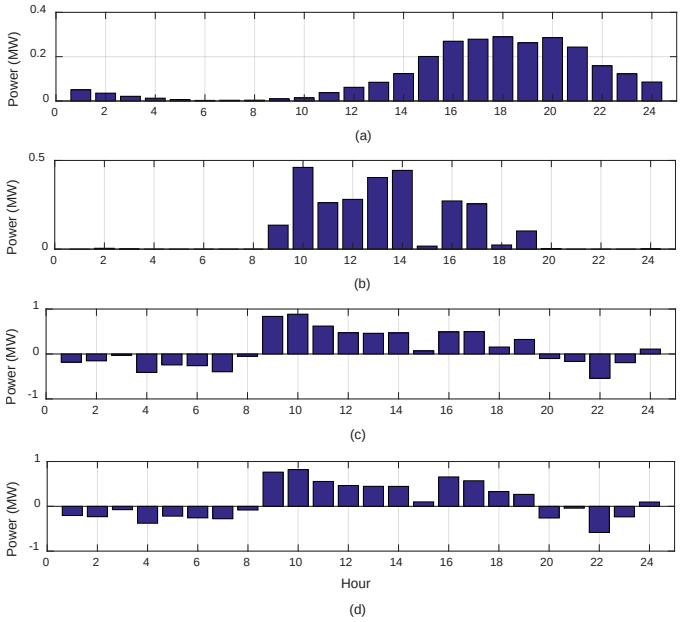

Fig. 6: Active power exchanges of the EV population for cases a) I, b) II, c) III and d) IV.

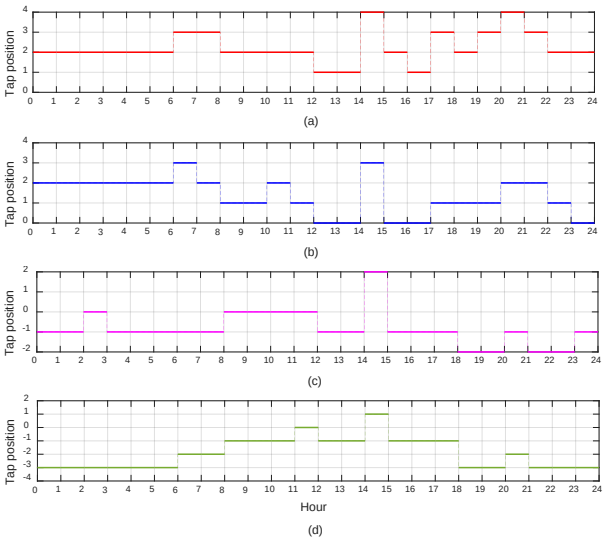

Fig. 7: OLTC tap positions for cases a) I, b) II, c) III and d) IV.

to lower positions as shown in Fig. 7. In case IV, the active power profile of the EV population is similar to that of case III. This indicates that allowing the EVs to supply reactive power does not interfere with their charging/discharging schedule. As illustrated in Fig. 8, the EV population exhibit primarily capacitive behavior throughout the day in order to achieve lower OLTC tap positions than in the other cases without violating the lower voltage limit. This means that when the OLTC tap is set to a lower position to steady decrease the voltage levels, the EVs inject reactive power into the grid to offset rapid voltage fluctuations that could lead to undervoltages.

Fig. 9 shows the voltage profiles for the three cases. Each boxplot summarizes for each bus the voltage magnitudes for

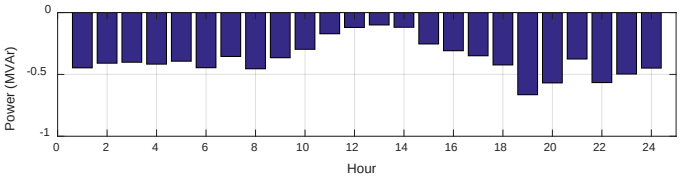

Fig. 8: Reactive power exchanged by the EV population in case IV

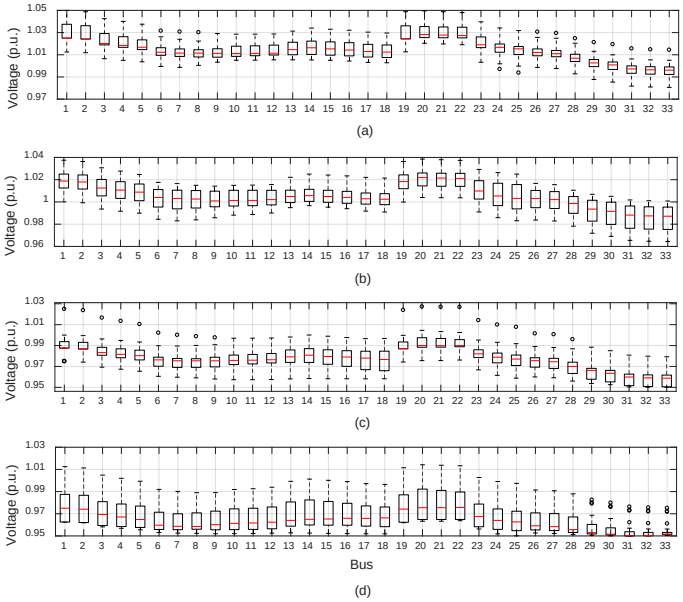

Fig. 9: Voltage profiles for cases a) I, b) II, c) III and d) IV.

the 24-hours period. In case I, the voltage levels remain above the nominal most of the time for most buses, reaching a minimum value of about 0.98 p.u. at bus 33. In case II, the voltage levels are lowered reaching a minimum value of about 0.96 p.u. at bus 33. In case III, it is possible to lower the voltage levels to values below the nominal most of the time for most buses. In this case the voltage levels reach a minimum value of 0.95 p.u. The active and reactive V2G capabilities of EVs in case IV have the most significant effect on decreasing the voltage levels in the EDS, resulting in several buses reaching voltage levels close or equal to the lower limit for several hours during the day.

C. Sensitivity analysis

The effect of different penetration levels of RES-based DG and EVs on the performance of CVR is evaluated in this subsection. For the tests performed in the previous subsection, the total RES-based DG installed capacity represents a penetration level of 107%, and the population of 318 EVs represents a penetration level of 60%. The CVR performance is now being evaluated for RES-based DG penetration levels of 53%, 107%, and 140% considering EV penetration levels of 20%, 40%, 60%, and 80%. These RES-based DG penetration levels represent low, medium, and high installed capacity scenarios, relative to the maximum capacity that can be accommodated in the EDS without violating operating limits. The maximum RES-based DG installed capacity that can be

TABLE II: Summary of the conventional load consumption and energy losses for different RES-based DG and EV penetration levels

Cases		Load (MWh)	Loss (MWh)	ΔLoad (%)	ΔLoss (%)
140% DG	20% EV	50.63	1.27	-	-
	40% EV	50.13	1.21	0.99	4.72
	60% EV	49.79	1.17	1.66	7.87
	80% EV	49.68	1.17	1.88	7.87
107% DG	20% EV	50.72	1.02	-	-
	40% EV	50.17	0.98	1.08	3.92
	60% EV	49.90	0.98	1.62	3.92
	80% EV	49.64	0.98	2.13	3.92
53% DG	20% EV	51.05	1.05	-	-
	40% EV	50.49	1.06	1.10	-0.95
	60% EV	50.02	1.06	2.02	-0.95
	80% EV	49.80	1.07	2.45	-1.90

accommodated in the EDS was estimated using the hosting capacity analysis described in [17] and corresponds to a penetration level of around 140%. A summary of the results for case III is presented in Table 2. Columns 3 and 4 show the percentage changes in conventional load consumption and energy losses, respectively. These changes are obtained by comparing the values of conventional load consumption and energy losses of the scenario with 20% EV penetration level with those of the other scenarios.

As the EV penetration level increases from 20% to 80%, the trend is to obtain smaller reductions in conventional load consumption with larger RES-based DG penetration levels. For instance, with a 140% RES-based DG penetration level, reductions in conventional load consumption range from 0.99% to 1.88%, whereas with a 53% penetration level, reductions range from 1.10% to 2.45%. On the other hand, higher reductions in energy losses are obtained with higher RES-based DG penetration levels. When the RES-based DG penetration level is 140%, up to 7.87% energy loss reduction is achieved, whereas with a 53% RES-based DG penetration level, energy losses actually increase. Substantial reductions on energy losses are obtained by increasing the EV penetration level in the scenario with 140% RES-based DG penetration level because the EV population locally consume the energy supplied by the DG, which reduces the energy flowing larger distances to the substation. With 53% RES-based DG penetration level, the energy losses increase with higher EV penetration levels because more energy has to be transported from the substation to meet the EV demand.

V. Conclusions

A Volt-Var optimization model that includes the coordinated active and reactive power dispatch of aggregated EVs for CVR implementation in MV EDSs was proposed. EVs were model as clustered at specific EDS nodes taking into account technical characteristics and the driving pattern of individual EVs. Uncertainties related to prediction errors of solar PV and wind-based DG power production, conventional load consumption and EV driving patterns were taken into account through a two-stage stochastic programming formulations. Results showed that by including the coordinated dispatch of EVs is possible to obtain deeper voltage reductions than with the OLTC operating alone, which translates in higher energy savings. About 4.14% of energy savings were obtained coordinating the active and reactive power absorbed and injected by a population of 318 EVs. As future work, it is intended to carry out an exhaustive study that evaluates the effect of different categories of electric vehicles with different consumption patterns on the implementation of CVR. Examples of EV categories include goods-carrying EVs, extended range EVs, and passenger EVs.

References

[1] A. Padilha-Feltrin, D. A. Quijano Rodezno, and J. R. S. Mantovani, "Volt-var multiobjective optimization to peak-load relief and energy efficiency in distribution networks," *IEEE Trans. Power Del.*, vol. 30, no. 2, pp. 618–626, 2015.

[2] Z. Wang and J. Wang, "Time-varying stochastic assessment of conservation voltage reduction based on load modeling," *IEEE Trans. Power Syst.*, vol. 29, no. 5, pp. 2321–2328, 2014.

[3] ——, "Review on implementation and assessment of conservation voltage reduction," *IEEE Trans. Power Syst.*, vol. 29, no. 3, pp. 1306–1315, 2014.

[4] D. A. Quijano and A. Padilha-Feltrin, "Optimal integration of distributed generation and conservation voltage reduction in active distribution networks," *Int. J. Electr. Power Energy Syst.*, vol. 113, pp. 197–207, 2019.

[5] R. W. Uluski, "Vvc in the smart grid era," in *IEEE PES General Meeting*, 2010, pp. 1–7.

[6] Q. Zhang, K. Dehghanpour, and Z. Wang, "Distributed cvr in unbalanced distribution systems with pv penetration," *IEEE Trans. Smart Grid*, vol. 10, no. 5, pp. 5308–5319, 2019.

[7] S. Singh, V. Babu Pamshetti, A. K. Thakur, and S. P. Singh, "Multistage multiobjective volt/var control for smart grid-enabled cvr with solar pv penetration," *IEEE Syst. J.*, vol. 15, no. 2, pp. 2767–2778, 2021.

[8] Y. Zhang, Y. Xu, H. Yang, and Z. Y. Dong, "Voltage regulation-oriented co-planning of distributed generation and battery storage in active distribution networks," *Int. J. Electr. Power Energy Syst.*, vol. 105, pp. 79–88, 2019.

[9] D. Choeum and D.-H. Choi, "Vulnerability assessment of conservation voltage reduction to load redistribution attack in unbalanced active distribution networks," *IEEE Trans. Ind. Informat.*, vol. 17, no. 1, pp. 473–483, 2021.

[10] M. S. Hossan and B. Chowdhury, "Integrated cvr and demand response framework for advanced distribution management systems," *IEEE Trans. Sustain. Energy*, vol. 11, no. 1, pp. 534–544, 2020.

[11] A. Dutta, S. Ganguly, and C. Kumar, "Mpc-based coordinated voltage control in active distribution networks incorporating cvr and dr," *IEEE Trans. Ind. Appl.*, vol. 58, no. 4, pp. 4309–4318, 2022.

[12] V. B. Pamshetti, S. Singh, A. K. Thakur, and S. P. Singh, "Multistage coordination volt/var control with cvr in active distribution network in presence of inverter-based dg units and soft open points," *IEEE Trans. Ind. Appl.*, vol. 57, no. 3, pp. 2035–2047, 2021.

[13] F. Teng, Z. Ding, Z. Hu, and P. Sarikprueck, "Technical review on advanced approaches for electric vehicle charging demand management, part i: Applications in electric power market and renewable energy integration," *IEEE Tran. Ind. Appl.*, vol. 56, no. 5, pp. 5684–5694, 2020.

[14] S. Li, C. Gu, J. Li, H. Wang, and Q. Yang, "Boosting grid efficiency and resiliency by releasing v2g potentiality through a novel rolling prediction-decision framework and deep-lstm algorithm," *IEEE Syst. J.*, vol. 15, no. 2, pp. 2562–2570, 2021.

[15] N. I. Nimalsiri, E. L. Ratnam, D. B. Smith, C. P. Mediwaththe, and S. K. Halgamuge, "Coordinated charge and discharge scheduling of electric vehicles for load curve shaping," *IEEE Trans. Intell. Transp. Syst.*, vol. 23, no. 7, pp. 7653–7665, 2022.

[16] X. Chen and K.-C. Leung, "Non-cooperative and cooperative optimization of scheduling with vehicle-to-grid regulation services," *IEEE Trans. Veh. Technol.*, vol. 69, no. 1, pp. 114–130, 2020.

[17] D. A. Quijano, O. D. Melgar-Dominguez, C. Sabillon, B. Venkatesh, and A. Padilha-Feltrin, "Increasing distributed generation hosting capacity in distribution systems via optimal coordination of electric vehicle aggregators," *IET Gener., Trans. Dist.*, vol. 15, no. 2, pp. 359–370, 2021.

[18] M. C. Kisacikoglu, B. Ozpineci, and L. M. Tolbert, "Examination of a phev bidirectional charger system for v2g reactive power compensation," in *2010 Twenty-Fifth Annual IEEE Applied Power Electronics Conference and Exposition (APEC)*, 2010, pp. 458–465.

[19] J. Singh and R. Tiwari, "Cost benefit analysis for v2g implementation of electric vehicles in distribution system," *IEEE Trans. Ind. Appl.*, vol. 56, no. 5, pp. 5963–5973, 2020.
[20] J. Hu, C. Ye, Y. Ding, J. Tang, and S. Liu, "A distributed mpc to exploit reactive power v2g for real-time voltage regulation in distribution networks," *IEEE Trans. Smart Grid*, vol. 13, no. 1, pp. 576–588, 2022.
[21] S. Singh, V. B. Pamshetti, and S. P. Singh, "Time horizon-based model predictive volt/var optimization for smart grid enabled cvr in the presence of electric vehicle charging loads," *IEEE Trans. Ind. Appl.*, vol. 55, no. 6, pp. 5502–5513, 2019.
[22] H. Gharavi, G. McLorn, X. Liu, and S. McLoone, "Coordinating ev charging and dynamic cvr in a lv network: A uk case study," *IFAC-PapersOnLine*, vol. 51, no. 10, pp. 193–198, 2018.
[23] X. Gao, G. De Carne, M. Andresen, S. Brske, S. Pugliese, and M. Liserre, "Voltage-dependent load-leveling approach by means of electric vehicle fast charging stations," *IEEE Trans. Transp. Electrification*, vol. 7, no. 3, pp. 1099–1111, 2021.
[24] D. A. Quijano, A. Padilha-Feltrin, and J. P. S. Catalo, "Volt-var optimization with power management of plug-in electric vehicles for conservation voltage reduction in distribution systems," in *2022 IEEE International Conference on Environment and Electrical Engineering and 2022 IEEE Industrial and Commercial Power Systems Europe (EEEIC / I&CPS Europe)*, 2022, pp. 1–6.
[25] M. Baran and F. Wu, "Network reconfiguration in distribution systems for loss reduction and load balancing," *IEEE Trans. Power Del.*, vol. 4, no. 2, pp. 1401–1407, 1989.
[26] L. Gan, N. Li, U. Topcu, and S. H. Low, "Exact convex relaxation of optimal power flow in radial networks," *IEEE Trans. Autom. Control*, vol. 60, no. 1, pp. 72–87, 2015.
[27] H. Bludszuweit, J. A. Dominguez-Navarro, and A. Llombart, "Statistical analysis of wind power forecast error," *IEEE Transactions on Power Systems*, vol. 23, no. 3, pp. 983–991, 2008.
[28] W. Yao, J. Zhao, F. Wen, Y. Xue, and G. Ledwich, "A hierarchical decomposition approach for coordinated dispatch of plug-in electric vehicles," *IEEE Transactions on Power Systems*, vol. 28, no. 3, pp. 2768–2778, 2013.
[29] H. Heitsch and W. Römisch, "Scenario reduction algorithms in stochastic programming," *Comput. Optim. Appl.*, vol. 24, no. 2, 2003.
[30] PodPoint, "Electric vehicle guide." Accessed February. 27, 2022. [Online]. Available: https://pod-point.com/guides/vehicles?